photonics

MDPI

Article

Equivalent Circuit Model of High-Performance VCSELs

Marwan Bou Sanayeh [1], Wissam Hamad [2,*] and Werner Hofmann [2]

[1] ECCE Department, Faculty of Engineering, Notre Dame University, P.O. Box 72 Zouk Mikael, Lebanon; mbousanayeh@ndu.edu.lb

[2] Institute of Solid State Physics and Center of Nanophotonics, Technical University of Berlin, Hardenbergstr. 36, 10623 Berlin, Germany; werner.hofmann@tu-berlin.de

* Correspondence: w.hamad@tu-berlin.de

Received: 12 December 2019; Accepted: 15 January 2020; Published: 18 January 2020

Abstract: In this work, a general equivalent circuit model based on the carrier reservoir splitting approach in high-performance multi-mode vertical-cavity surface-emitting lasers (VCSELs) is presented. This model accurately describes the intrinsic dynamic behavior of these VCSELs for the case where the lasing modes do not share a common carrier reservoir. Moreover, this circuit model is derived from advanced multi-mode rate equations that take into account the effect of spatial hole-burning, gain compression, and inhomogeneity in the carrier distribution between the lasing mode ensembles. The validity of the model is confirmed through simulation of the intrinsic modulation response of these lasers.

Keywords: high-speed VCSELs; multi-mode VCSELs; intrinsic laser dynamics; equivalent circuit modeling; intrinsic modulation response

1. Introduction

Vertical-cavity surface-emitting lasers (VCSELs) offer an excellent solution for many high-speed data communication challenges. Moreover, VCSELs have special features such as high integration level, low electrical power consumption, low divergence angle, simple packaging, low fabrication cost, high modulation speed at low currents, and good beam quality. These features led to the growth of the VCSEL market for a wide variety of applications, which are not only limited to the field of communications but also extends to consumer applications such as laser printers and optical mice [1,2]. Nowadays, despite the intensive research conducted to understand the underlying physics behind the multi-mode (MM) behavior in oxide-confined MM VCSELs and their impact on the intrinsic laser dynamics, many ambiguities still exist concerning the nature of the abnormal multi-peak phenomenon and the notches occurring in the small-signal modulation response of these VCSELs. These multiple local maxima which appear in their intrinsic dynamic response deviate substantially from the standard single-mode (SM) model normally applied to characterize these MM devices. The measured total small-signal modulation response of a laser is the result of the superposition of the intrinsic and the extrinsic responses. The need to accurately de-embed and analyze the intrinsic laser dynamic behavior of VCSELs becomes indispensable to understand and study their extrinsic chip behavior. However, since the intrinsic response is attributed to the structure and geometry of the VCSEL intrinsic region and lasing cavity, the only way to isolate its effects is by accurately modeling it. Hence, sufficient modeling and accurate parameter extraction strategies are needed for a reliable de-embedding approach of each of the intrinsic and extrinsic responses from the overall system response. This detailed understanding of the VCSELs modulation response enables further optimization of these lasers for next generation

high-speed devices. Furthermore, analyzing and modeling these lasers enable the enhancement and optimization of their design and performance.

Recently, an advanced and accurate MM small-signal model, which is based on the carrier reservoir splitting approach, was developed [3,4]. This rate equation-based model enables the extraction of reliable information from the intrinsic dynamics of high-speed MM VCSELs, as it takes into account the effect of spatial hole-burning (SHB), gain compression, and inhomogeneity in the carrier distribution between the modes. Using these MM rate equations also ensures deeper understanding of the device MM laser dynamics and gives a better access to the nonlinear modal competition behavior for the carrier density in the active region for such high-performance VCSELs.

Accurate modeling is important for both device engineers and circuit designers. Device engineers require a model that simulates complex physical phenomena, resulting in long and complex simulation times, and circuit designers need a simple and relatively accurate model that can be implanted in a circuit simulator and drivers with fast computational time. Hence, detailed analysis of VCSEL operating characteristics is crucial to the design of high-speed optical links. Traditionally, the intrinsic dynamics of a laser have been analyzed using a direct solution of the rate equations. This method gives accurate results; however, it has some disadvantages as numerical optimization techniques that minimizes the difference between measured and modeled data can vary depending upon the optimization method and starting values and as the device–circuit interaction cannot be easily taken into account [5]. An alternative approach to that of using the rate equations to model the VCSELs' intrinsic dynamics is to transform these equations to an equivalent circuit model, in which electrical components model the different physical effects that contribute to the overall system response [5–8]. This technique presents several advantages, including that the circuit model gives an intuitive idea of the physics of the device and the modulation response and can be easily interfaced to the VCSEL standard parasitic network [5,8].

Circuit modeling includes an electronic and an optical part and permits the optimization of the devices' dynamic characteristics including the device–circuit interaction, and performance can be obtained using a general circuit simulator. For example, to improve the f_{3dB} intrinsic modulation bandwidth of VCSELs, an intrinsic equivalent circuit model can be employed to accurately simulate the dynamic behavior inside the laser cavity and to understand in depth the effect of each device physical element on this intrinsic 3-dB frequency. Thus, using this advanced model and bearing in mind the relation between the circuit elements and the real word physical device layout, various simulations can be conducted by altering the values of some circuit components and by tracking the change in the resulting intrinsic 3-dB bandwidth. It was noticed that, inside our latest generation of MM VCSELs with highest carrier and photon densities, the common carrier reservoir splits up as a result of numerous effects such as mode competition, carrier diffusion, and SHB. Besides the well-understood mechanisms which control the strength and the form of relaxation oscillation frequency (e.g., carrier diffusion, nonlinear gain suppression, and carrier transport effects), the contribution of codominant higher-order modes is still under discussion. In general, these VCSELs are fabricated with a small circular aperture diameter, allowing only few modes to rise under operation. Hence, most of these transverse lasing modes are spatially localized in two main regions and therefore can be confined either in the center of the active region or are localized more towards the peripheral boundary of the carrier reservoir. Constituently, these lasing modes can be grouped into two mode ensembles: the central mode ensemble and the peripheral mode ensemble. For SM VCSELs, the solution of the rate equations is straight forward and the fitting procedure for parameter extraction is simple. For MM VCSELS, however, and as shown in Reference [4], even for two-mode ensembles, the analysis becomes very complex and the parameter extraction and development of an analytical intrinsic modulation expression becomes rigorous.

In this work, a general compact and comprehensive equivalent circuit model for MM VCSELs, which is based on our latest novel MM rate equations model, i.e., the carrier reservoir splitting approach, is presented. This circuit model has all the advantages of simple and fast simulation procedures of

circuit modeling and still incorporates advanced features of lasing modes interactions given by the advanced MM rate equations model. Most importantly, the proposed equivalent circuit model can reproduce the delicate measured intrinsic modulation response. The validity of the model is confirmed through simulations and plots of the intrinsic modulation response of a two-mode ensembles VCSEL equivalent circuit model. These simulation results are later compared to the experimentally measured intrinsic modulation response of our high-performance VCSELs.

2. Rate Equations

Small-signal advanced MM rate equations for high-speed MM VCSELs, which are based on mode competition for carrier density in the active region, were recently developed [3,4]. In order to map these rate equations to the proposed equivalent circuit model, we quickly review the different derivation steps leading to the system's intrinsic modulation response and interaction matrices. We first linearize a system of differential equations that represent the rates of change in the carrier and photon reservoir densities and rewrite them to get the rate coefficients above lasing threshold, which are

$$\mu_{NiNi} = \delta J_{th_i} / \delta N_i + v_g a_i S_i \tag{1}$$

$$\mu_{NiSi} = v_g g_{th_i} - v_g a_{p_i} S_i \tag{2}$$

$$\mu_{SiNi} = \Gamma_i v_g a_i S_i \tag{3}$$

$$\mu_{SiSi} = \Gamma_i v_g a_{p_i} S_i \tag{4}$$

where i represents the ith mode in the corresponding carrier or photon reservoirs; g_{thi} is the gain at threshold; a_i and a_{pi} are the differential gain and the negative gain derivatives, respectively; N_i is the carrier density; and S_i is the photon density in the active region and the optical cavity. Moreover, Γ_i is the confinement factor, v_g is the group velocity, and J_{thi} is the carrier recombination density due to spontaneous emission or losses. The system's relaxation oscillation frequency ω_{Ri} and the damping factor γ_i in terms of the simplified rate coefficients can be introduced as

$$\omega_{Ri}^2 = \mu_{NiNi}\mu_{SiSi} + \mu_{NiSi}\mu_{SiNi} \tag{5}$$

$$\gamma_i = \mu_{NiNi} + \mu_{SiSi} \tag{6}$$

For SM VCSELs, the resulting rate coefficients can be expressed in a matrix form as

$$\begin{pmatrix} j\omega + \mu_{NN} & \mu_{NS} \\ -\mu_{SN} & j\omega + \mu_{SS} \end{pmatrix} \begin{pmatrix} dN \\ dS \end{pmatrix} = \begin{pmatrix} dJ \\ 0 \end{pmatrix} \tag{7}$$

where J is the driving current density. For MM VCSELs, the matrix representation of the SM model can be expanded to include the various interactions between the different carrier and photon reservoirs. When expanded, the matrix representation for the case of two lasing modes ensembles, which is for most purposes sufficient to describe the intrinsic dynamics of the reservoir splitting in MM VCSELs, is expressed as

$$\begin{pmatrix} j\omega + \mu_{N_1N_1} & \mu_{N_1N_2} & \mu_{N_1S_1} & \mu_{N_1S_2} \\ \mu_{N_2N_1} & j\omega + \mu_{N_2N_2} & \mu_{N_2S_1} & \mu_{N_2S_2} \\ -\mu_{S_1N_1} & 0 & j\omega + \mu_{S_1S_1} & 0 \\ 0 & -\mu_{S_2N_2} & 0 & j\omega + \mu_{S_2S_2} \end{pmatrix} \begin{pmatrix} dN_1 \\ dN_2 \\ dS_1 \\ dS_2 \end{pmatrix} = \begin{pmatrix} dJ_1 \\ dJ_2 \\ 0 \\ 0 \end{pmatrix} \tag{8}$$

The interaction between the two carrier reservoir densities N_1 and N_2 can be written as shown in Equations (9) and (10), where s_{12} and s_{21} represent the spatial dependency of the two interacting carrier reservoirs.

$$\mu_{N1N2} = s_{21} \cdot v_g a S_2 \simeq s_{21} \cdot \mu_{N2N2} \tag{9}$$

$$\mu_{N2N1} = s_{12} \cdot v_g a S_1 \simeq s_{12} \cdot \mu_{N1N1} \tag{10}$$

Similarly, the interaction coefficients representing cross reabsorption can be written as

$$\mu_{N1S2} = s_{21} \cdot v_g a g_{th2} = s_{21} \cdot \mu_{N2S2} \tag{11}$$

$$\mu_{N2S1} = s_{12} \cdot v_g a g_{th1} = s_{12} \cdot \mu_{N1S1} \tag{12}$$

For a system having any number of mode ensembles (m-mode ensembles), the matrix in Equation (8) can be further expanded and generalized into the interaction matrix shown in Equation (13).

$$\begin{pmatrix} j\omega + \mu_{N_1N_1} & \cdots & \mu_{N_1N_n} & \mu_{N_1S_1} & \cdots & \mu_{N_1S_n} \\ \vdots & \ddots & \vdots & \vdots & \ddots & \vdots \\ \mu_{N_nN_1} & \cdots & j\omega + \mu_{N_nN_n} & \mu_{N_nS_1} & \cdots & \mu_{N_nS_n} \\ -\mu_{S_1N_1} & \cdots & -\mu_{S_1N_n} & j\omega + \mu_{S_1S_1} & \cdots & -\mu_{S_1S_n} \\ \vdots & \ddots & \vdots & \vdots & \ddots & \vdots \\ -\mu_{S_nN_1} & \cdots & -\mu_{S_nN_n} & \mu_{S_nS_1} & \cdots & j\omega + \mu_{S_nS_n} \end{pmatrix} \begin{pmatrix} dN_1 \\ \vdots \\ dN_n \\ dS_1 \\ \vdots \\ dS_n \end{pmatrix} = \begin{pmatrix} dJ_1 \\ \vdots \\ dJ_n \\ 0 \\ \vdots \\ 0 \end{pmatrix} \tag{13}$$

From the interaction matrices shown in Equations (7), (8) and (13), the intrinsic modulation responses of SM and MM VCSELs can be obtained. These can be used to model the intrinsic dynamics of VCSELs, but for MM VCSELs, they can be quite complicated to solve analytically and require either complex numerical calculations or the neglection of some minor physical effects. Alternatively, equivalent circuit modeling, presented in Section 3, can be adopted.

3. Equivalent Circuit Modeling

3.1. Review on the Single Mode Model

The standard equivalent electrical circuit model of a SM (single-mode) VCSEL intrinsic dynamic operation is shown in Figure 1, which is well established and can be found in different literatures [5,8]. This model can be easily integrated into the small-signal cascaded network model of the VCSEL diode that includes the source, cables, submout parasitics, and laser chip parasitics that represent the extrinsic laser dynamics (e.g., Figure 1 in Reference [8]). The different components in this circuit represent different elements of the rate equations. For example, the capacitance C is the sum of the space-charge capacitance of the heterojunction and the charge storage in the active layer. The small-signal photon storage is modeled by the inductance L. The small-signal photon density is proportional to the current over L and thus can be used as the output variable representing the optical output intensity. Using the interaction matrix in Equation (7), the intrinsic modulation response for SM VCSELs, $H_{SM}(\omega)$ is found as

$$H_{SM}(\omega) = \frac{h\nu}{e}\eta_d \frac{{\omega'_R}^2}{\omega_R^2 + j\omega\gamma - \omega^2} \tag{14}$$

where η_d is the differential quantum efficiency and ${\omega'_R}^2 = v_g g_{th} \mu_{SN}$. The relaxation oscillation frequency ω_R usually replaces ω'_R for standard physical device parameters and is a common approximation for the SM modulation approach [9]. By comparing the rate equation-based transfer function in Equation (14) with the calculated electrical transfer function of the circuit model shown in Figure 1, the latter can be written as

$$H_{SM,elec}(\omega) = \frac{I_{out}}{I_{in}} = \frac{1/LC}{1/LC + R_{1b}/LR_{1a}C + j\omega\left(1/R_{1a}C + R_{1b}/L\right) - \omega^2} \tag{15}$$

Comparing the two transfer functions, the interaction matrix in Equation (7) can be rewritten in term of its electrical circuit model equivalent, and the equivalencies acquired can be used afterwards to

develop the MM VCSEL equivalent circuit model. Equations (16a) and (16b) show the comparison between the rate equation-based matrix and its electrical circuit model equivalent:

$$\begin{pmatrix} j\omega+\mu_{NN} & \mu_{NS} \\ -\mu_{SN} & j\omega+\mu_{SS} \end{pmatrix}\begin{pmatrix} dN \\ dS \end{pmatrix}=\begin{pmatrix} dJ \\ 0 \end{pmatrix} \quad (\mathbf{a})$$
$$\updownarrow$$
$$\begin{pmatrix} j\omega+1/R_{1a}C & 1/L \\ -1/C & j\omega+R_{1b}/L \end{pmatrix}\begin{pmatrix} Cv_c/q \\ Li_L/q \end{pmatrix}=\begin{pmatrix} \eta_I dI/qV_o \\ 0 \end{pmatrix} \quad (\mathbf{b}) \tag{16}$$

where η_I is the electrical efficiency, v_c is the voltage over the capacitance, and i_L the current in the inductance. Moreover, $\eta_I dI/V_o$ is represented by the current source I_{so} in Figure 1. Solving the matrix in Equation (16b) leads to Equations (17) and (18):

$$j\omega\frac{Cv_c}{q}+\frac{v_c}{qR_{1a}}+\frac{i_L}{q}=\frac{\eta_I dI}{qV_o} \tag{17}$$

$$i_L=\frac{v_c}{R_{1b}+j\omega L} \tag{18}$$

Replacing i_L in Equation (17), the node equation of the circuit shown in Figure 1 can be obtained as

$$v_c j\omega C+\frac{v_c}{R_{1a}}+\frac{v_c}{R_{1b}+j\omega L}-\underbrace{\frac{\eta_I dI}{V_o}}_{I_{so}}=0 \tag{19}$$

This SM model resembles a simple second-order low-pass filter. Moreover, in most literatures, the adapted SM based equivalent circuit model can only reproduce a single resonance peak and thus fails to replicate the delicate small-signal data (abnormal multi-peaks and the notches) of modern high-speed MM VCSELs accurately.

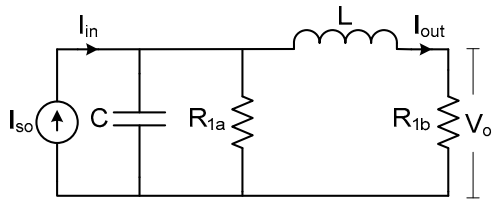

Figure 1. Standard equivalent electrical circuit model of a SM VCSEL intrinsic dynamic operation [5,8].

3.2. Two-Mode Model

To analyze the intrinsic behavior of high-performance MM VCSELs, a suitable equivalent circuit model is developed. In this section, we derive this model for a MM VCSEL having two mode ensembles. This model will be later expanded to comprise a system of any number of mode ensembles (Section 3.3). Using the relations in Equations (9)–(12) and the equivalencies that were extracted from Equation (16), the interaction matrix shown in Equation (8) is converted to its circuit model equivalent, shown in Equation (20).

$$\begin{pmatrix} j\omega+\frac{1}{R_{1a}C_1} & s_{21}\cdot\frac{1}{R_{2a}C_2} & \frac{1}{L_1} & s_{21}\cdot\frac{1}{L_2} \\ s_{12}\cdot\frac{1}{R_{1a}C_1} & j\omega+\frac{1}{R_{2a}C_2} & s_{12}\cdot\frac{1}{L_1} & \frac{1}{L_2} \\ -\frac{1}{C_1} & 0 & j\omega+\frac{R_{1b}}{L_1} & 0 \\ 0 & -\frac{1}{C_2} & 0 & j\omega+\frac{R_{2b}}{L_2} \end{pmatrix}\begin{pmatrix} \frac{C_1 v_{c1}}{q} \\ \frac{C_2 v_{c2}}{q} \\ \frac{L_1 i_{L1}}{q} \\ \frac{L_2 i_{L2}}{q} \end{pmatrix}=\begin{pmatrix} \frac{\eta_I dI_1}{qV_{o1}} \\ \frac{\eta_I dI_2}{qV_{o2}} \\ 0 \\ 0 \end{pmatrix} \tag{20}$$

Solving the matrix in Equation (20) leads to the following relations:

$$j\omega \cdot \frac{C_1 v_{c1}}{q} + \frac{v_{c1}}{R_{1a}q} + s_{21} \cdot \frac{v_{c2}}{R_{2a}q} + \frac{i_{L1}}{q} + s_{21} \cdot \frac{i_{L2}}{q} = \frac{\eta_I dI_1}{qV_{o1}} \tag{21}$$

$$j\omega \cdot \frac{C_1 v_{c1}}{q} + \frac{v_{c1}}{R_{1a}q} + s_{21} \cdot \frac{v_{c2}}{R_{2a}q} + \frac{i_{L1}}{q} + s_{21} \cdot \frac{i_{L2}}{q} = \frac{\eta_I dI_1}{qV_{o1}} \tag{22}$$

$$i_{L1} = \frac{v_{c1}}{R_{1b} + j\omega L_1} \tag{23}$$

$$i_{L2} = \frac{v_{c2}}{R_{2b} + j\omega L_2} \tag{24}$$

Replacing i_{L1} and i_{L2} in Equations (21) and (22), the node equations for the two-mode VCSEL model can be obtained as shown in Equations (25) and (26).

$$s_{21}\left(\frac{v_{c2}}{R_{2a}} + \underbrace{\frac{v_{c2}}{R_{2b} + j\omega L_2}}_{I_{12}}\right) + v_{c1} j\omega C_1 + \frac{v_{c1}}{R_{1a}} + \frac{v_{c1}}{R_{1b} + j\omega L_1} - \underbrace{\frac{\eta_I dI_1}{V_{o1}}}_{I_{so1}} = 0 \tag{25}$$

$$s_{12} \cdot \left(\frac{v_{c1}}{R_{1a}} + \underbrace{\frac{v_{c1}}{R_{1b} + j\omega L_1}}_{I_{21}}\right) + v_{c2} j\omega C_2 + \frac{v_{c2}}{R_{2a}} + \frac{v_{c2}}{R_{2b} + j\omega L_2} - \underbrace{\frac{\eta_I dI_2}{V_{o2}}}_{I_{so2}} = 0 \tag{26}$$

Using the node equations in Equations (25) and (26), the two-mode VCSEL equivalent circuit model can be obtained, as shown in Figure 2. In this circuit, we can consider, just like in the SM model, that $I_{so1} = \eta_I dI/V_{o1}$ and $I_{so2} = \eta_I dI/V_{o2}$ and that $s_{21}I_{12}$ and $s_{12}I_{21}$ are dependent current sources, which represent the interaction of the two carrier reservoirs with each other. This is an important aspect to consider, as it has been recently shown in MM VCSELs that the split carrier reservoirs of the lasing mode ensembles overlap and impact each other [3,4].

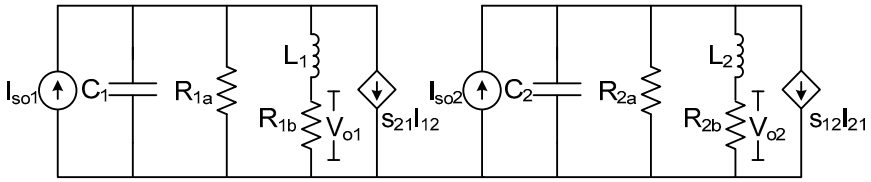

Figure 2. Equivalent electrical circuit model of a two-mode multi-mode VCSEL intrinsic dynamic operation.

3.3. M-Mode Model

Similar to the two-mode model equivalent circuit analysis, the electrical circuit equivalent matrix, shown in Equation (27), for a MM VCSEL with m-mode ensembles can be derived. From this matrix representation, the set of node equations (grouped in Equation (28)) can be obtained, following the same derivation procedure of the two-mode model case. Using these node equations, the m-mode equivalent electrical circuit model, depicted in Figure 3, can be developed.

$$\begin{pmatrix} j\omega + \frac{1}{R_{1a}C_1} & \cdots & s_{m1}\cdot\frac{1}{R_{ma}C_n} & \frac{1}{L_1} & \cdots & s_{m1}\cdot\frac{1}{L_1} \\ \vdots & \ddots & \vdots & \vdots & \ddots & \vdots \\ s_{1m}\cdot\frac{1}{R_{1a}C_1} & \cdots & j\omega + \frac{1}{R_{ma}C_m} & s_{1m}\cdot\frac{1}{L_1} & \cdots & \frac{1}{L_m} \\ -\frac{1}{C_1} & \cdots & 0 & j\omega + \frac{R_{1b}}{L_1} & \cdots & 0 \\ \vdots & \ddots & \vdots & \vdots & \ddots & \vdots \\ 0 & \cdots & -\frac{1}{C_m} & 0 & \cdots & j\omega + \frac{R_{mb}}{L_n} \end{pmatrix} \begin{pmatrix} \frac{C_1 v_{c1}}{q} \\ \vdots \\ \frac{C_m v_{cm}}{q} \\ \frac{L_1 i_{L1}}{q} \\ \vdots \\ \frac{L_m i_{Lm}}{q} \end{pmatrix} = \begin{pmatrix} \frac{\eta_i dI_1}{qV_{o1}} \\ \vdots \\ \frac{\eta_i dI_m}{qV_{om}} \\ 0 \\ \vdots \\ 0 \end{pmatrix} \tag{27}$$

$$\begin{aligned} &\sum_{i=2}^{m} s_{i1}\cdot\Big(\underbrace{\tfrac{v_{ci}}{R_{ia}} + \tfrac{v_{ci}}{R_{ib}+j\omega L_i}}_{I_{1i}}\Big) + v_{c1}\,j\omega C_1 + \tfrac{v_{c1}}{R_{1a}} + \tfrac{v_{c1}}{R_{1b}+j\omega L_1} - \underbrace{\tfrac{\eta_I dI_1}{V_{o1}}}_{I_{so1}} = 0 \\ &\qquad\qquad \vdots \\ &\sum_{i=1}^{m-1} s_{im}\cdot\Big(\underbrace{\tfrac{v_{ci}}{R_{ia}} + \tfrac{v_{ci}}{R_{ib}+j\omega L_i}}_{I_{mi}}\Big) + v_{cm}\,j\omega C_m + \tfrac{v_{cm}}{R_{ma}} + \tfrac{v_{cm}}{R_{mb}+j\omega L_m} - \underbrace{\tfrac{\eta_I dI_m}{V_{om}}}_{I_{som}} = 0 \end{aligned} \tag{28}$$

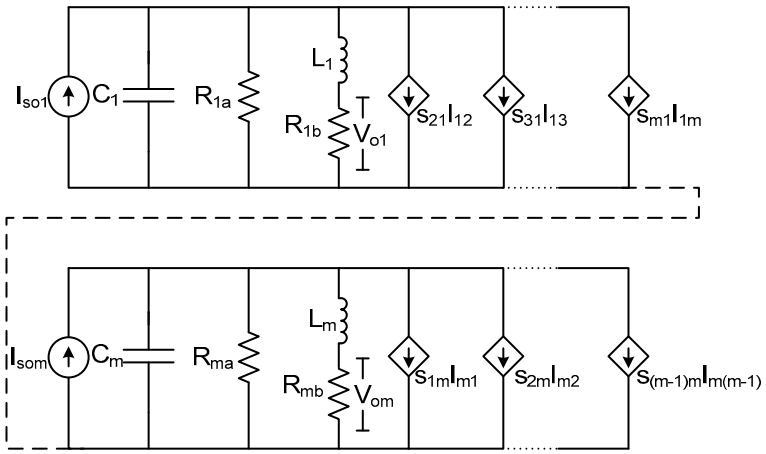

Figure 3. Equivalent electrical circuit model for an m-mode multi-mode VCSEL intrinsic dynamic operation.

4. Circuit Simulation Results

In order to derive the total small-signal modulation response $H_{TOT}(\omega)$ of a MM VCSEL, its intrinsic transfer function $H_{int}(\omega)$ is multiplied by the extrinsic transfer function of its parasitic network $H_{par}(\omega)$. This extrinsic response was recently developed for high-performance MM VCSELs [10]. In physical real-world devices, the intrinsic dynamic behavior is usually embedded in such a cascaded network that includes different parasitic elements, such as the submount and laser chip parasitics. The laser chip parasitics, also called the extrinsic response, play one of the most critical roles in limiting the intrinsic modulation speed, as their low-pass filter characteristics shunts the modulation current outside the active region at high frequencies and since the extrinsic response is attributed to the structure and geometry of the VCSEL chip; the only way to isolate its effects is by modeling it with an electrical equivalent circuit, of which electrical components represent the different physical effects that contribute to the overall system response. Having an equivalent circuit for the intrinsic response, as shown in this work, enables the combination of both the extrinsic and intrinsic modulation responses in the overall cascaded network of the entire link. Figure 4 shows the calibrated total small-signal modulation response of a 980-nm MM oxide-confined VCSEL with an aperture diameter of ~7 μm measured by a

40-GHz vector network analyzer (VNA-HP8722C). The curves describe the measured total relative modulation response data S_{21} for various driving currents at room temperature. The modulation current is increased gradually up to 14 mA. Thermal rollover is reached at around 17 mA. The maximum total 3-dB bandwidth of the device including chip parasitics is found to exceed 32 GHz at 14 mA.

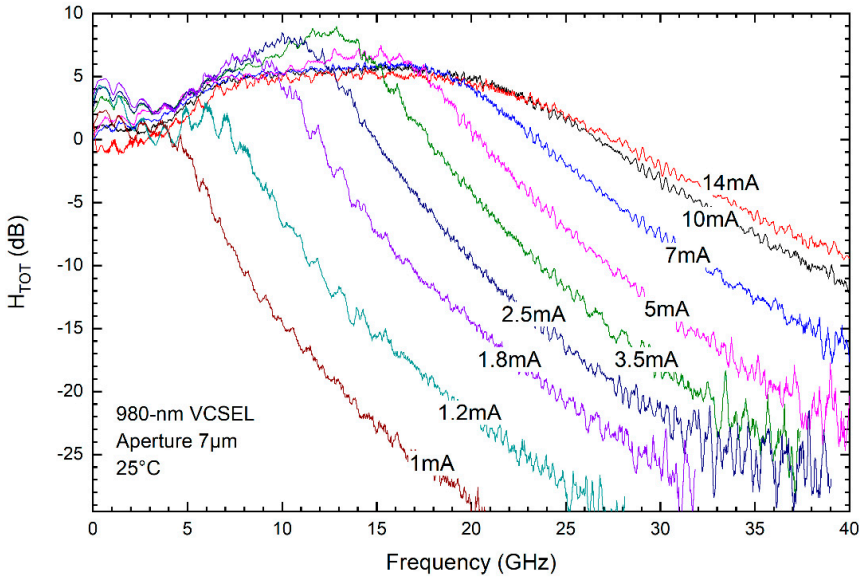

Figure 4. Calibrated total (intrinsic and extrinsic) small-signal modulation response of a 980-nm MM oxide-confined VCSEL with an aperture diameter of ~7 μm: The curves depict the measured relative response data (S_{21}) for various driving currents at room temperature.

In order to de-embed the pure intrinsic modulation response $H_{int}(\omega)$ from the total modulation response, either the direct rate equations solution or the proposed equivalent circuit model derived in this work can be used. As shown in Reference [4], even though it is very accurate, the calculated $H_{int}(\omega)$ is very complex to implement and an advanced fitting procedure is required to determine its physical parameters. Alternatively, the equivalent circuit model presented in this work has fewer fitting parameters compared to the rate equation model on one side, and secondly, it can be easily integrated in the overall system cascaded network.

To validate the proposed MM equivalent circuit model, MATLAB Simulink® was used to compute the intrinsic modulation response of the two-mode ensembles VCSEL circuit model shown in Figure 2. Results are presented in Figure 5 for three different driving currents. The curves represent the pure intrinsic small-signal modulation response of a two-mode ensembles VCSEL. The values of the circuit parameters used in this simulation are shown in the inset of Figure 5. These are a set of possible mathematical solutions that were extracted from fitting the intrinsic modulation response of the circuit model into its measured counterpart depicted in Figure 4. The parameter n shown in the inset of Figure 5 represents the injection current inhomogeneity factor, i.e., n and $1 - n$ are the fractions of the injection carrier densities in each carrier reservoir, and values have been experimentally determined in Reference [4] for different currents. In the model shown in Figure 2, this parameter will distribute the total current on I_{so1} and I_{so2} accordingly. This represents the inhomogeneity in the injection current distribution between the lasing mode ensembles. For the first two mode ensembles (LP_{01} and LP_{11}), s_{12} = 0.67 and s_{21} = 0.94 and were adopted from Reference [11]. At this point, it is important to mention that the chip-parasitics $H_{par}(\omega)$ need to be de-embedded from the total measured small-signal modulation response before comparing it to the simulated pure intrinsic response shown in Figure 5. As shown in Figure 5, the intrinsic small-signal modulation response replicates a typical MM VCSEL intrinsic response with the multi-peaks and notches in the curves at low frequencies. It is worth noting that the advanced circuit for a two-mode ensembles VCSEL depicted in Figure 2 shows a much more

realistic modulation response of MM VCSELs compared to using the SM VCSEL circuit in Figure 1, which was traditionally used in various literatures. Using the SM intrinsic modulation response model (Equation (14)) is acceptable as an approximation for low-speed MM VCSELs sharing the same carrier reservoir. However, in high-speed and high-performance VCSELs, using this simple model gives rise to a lot of discrepancies when modeling the intrinsic performance of these MM VCSELs [3,4].

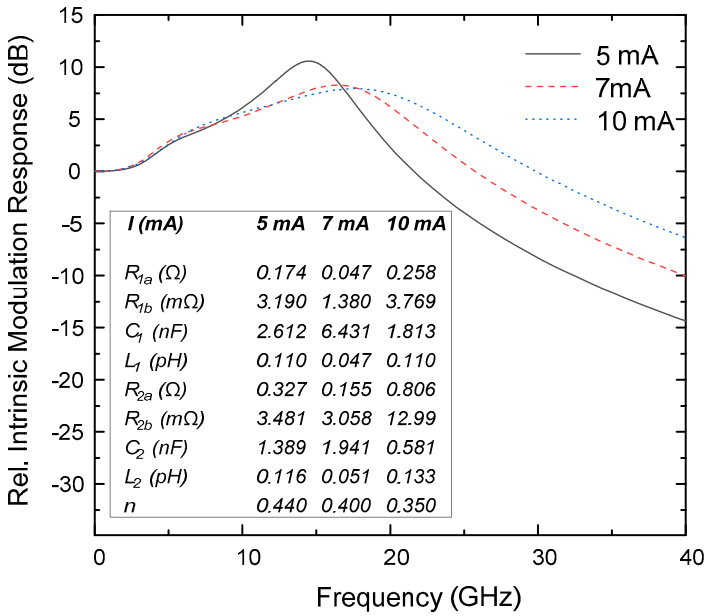

Figure 5. Simulation results of the relative intrinsic modulation response for three different driving currents using the two-mode VCSEL equivalent circuit model shown in Figure 2. Inset: testing parameters used in the two-mode VCSEL equivalent circuit model simulation.

5. Conclusions

In this study, a general, compact, and comprehensive equivalent circuit model based on the carrier reservoir splitting approach and that accurately describes the intrinsic dynamic behavior of MM VCSELs was presented. The model includes the case where the lasing modes do not share a common carrier reservoir and was derived from advanced MM rate equations that take into account the effect of spatial hole-burning, gain compression, and inhomogeneity in the carrier distribution into the different lasing modes. The validity of the model was confirmed through simulations of the intrinsic modulation response of a VCSEL having two lasing mode ensembles at different driving currents compared to measured data. This model can be expanded to include any number of mode ensembles. Moreover, this equivalent circuit model can be easily integrated in the overall system cascaded network that represents the extrinsic and intrinsic dynamics of MM VCSELs.

Author Contributions: Supervision, Writing—review & editing: M.B.S., W.H. (Wissam Hamad) and W.H. (Werner Hofmann). All authors have read and agreed to the published version of the manuscript.

Funding: This work was supported in part by the Erasmus+ programme and the German Research Foundation (DFG) within the Collaborative Research Center "Semiconductor Nanophotonics" (CRC 787) and the Open Access Publication Fund of TU Berlin.

Acknowledgments: The authors would like to thank (in alphabetical order) Bassel Aboul-Hosn, Oliver Daou, Elio Nakhle, and Rami Yehia for their valuable support within this research.

Conflicts of Interest: The authors declare no conflict of interest.

References

1. Larsson, A. Advances in VCSELs for Communication and Sensing. *IEEE J. Sel. Top. Quantum Electron.* **2011**, *17*, 1552–1567. [CrossRef]

2. Hofmann, W.; Bimberg, D. VCSEL-Based Light Sources—Scalability Challenges for VCSEL-Based Multi-100-Gb/s Systems. *IEEE Photonics J.* **2012**, *4*, 1831–1843. [CrossRef]
3. Hamad, W.; Wanckel, S.; Hofmann, W.H.E. Small-Signal Analysis of Ultra-High-Speed Multi-Mode VCSELs. *IEEE J. Quantum Electron.* **2016**, *52*, 1–11. [CrossRef]
4. Hamad, W.; Sanayeh, M.B.; Siepelmeyer, T.; Hamad, H.; Hofmann, W. Small-Signal Analysis of High-Performance VCSELs. *IEEE Photonics J.* **2019**, *11*, 1–12. [CrossRef]
5. Gao, J. High Frequency Modeling and Parameter Extraction for Vertical-Cavity Surface Emitting Lasers. *J. Lightwave Technol.* **2012**, *30*, 1757–1763. [CrossRef]
6. Tucker, R.S.; Pope, D.J. Microwave Circuit Models of Semiconductor Injection Lasers. *IEEE Trans. Microw. Theory Tech.* **1983**, *31*, 289–294. [CrossRef]
7. Marozsák, T. Circuit Model for Multiple Transverse Mode Vertical-Cavity Surface-Emitting Lasers. *J. Lightwave Technol.* **2003**, *21*, 2977–2982. [CrossRef]
8. Gao, J.; Li, X.; Flucke, J.; Boeck, G. Direct parameter-extraction method for laser diode rate-equation model. *J. Lightwave Technol.* **2004**, *22*, 1604–1609. [CrossRef]
9. Coldren, L.A.; Corzine, S.W.; Mashanovitch, M.L. Dynamic Effects. In *Diode Lasers and Photonic Integrated Circuits*, 2nd ed.; John Wiley & Sons: Somerset, NJ, USA, 2012.
10. Hamad, W.; Sanayeh, M.B.; Hamad, M.; Hofmann, W. Impedance Characteristics and Chip-Parasitics Extraction of High-Performance VCSELs. *IEEE J. Quantum Electron.* **2020**, *56*, 1–11. [CrossRef]
11. Valle, A.; Pesquera, L. Theoretical calculation of relative intensity noise of multimode vertical-cavity surface-emitting lasers. *IEEE J. Quantum Electron.* **2004**, *40*, 597–606. [CrossRef]